Effects of Precipitation on the Thermodynamic Structure of the Trade Wind Boundary Layer

BRUCE A. ALBRECHT

Department of Meteorology and Earth System Science Center, The Pennsylvania State University, University Park

A model of the thermodynamic structure of the trade wind boundary layer is formulated to include the parameterization of precipitation in relatively shallow clouds. Although the area-averaged simulated precipitation rates are relatively small (less than 1 mm/day), the inclusion of precipitation has an appreciable effect on the predicted thermodynamic structure. The cloud layer structure simulated with precipitation is warmer, drier, and more stable than that simulated without precipitation. The simulated inversion height is lowered by as much as 60 mbar when precipitation is included.

1. INTRODUCTION

Shallow cumulus clouds are present over a large fraction of the world's oceans. Advection, convection, and radiation maintain a characteristic thermodynamic structure with a cloud layer that is often capped by an inversion of sufficient strength to inhibit deep convection.

Although the shallow clouds observed during undisturbed conditions are often considered to be nonprecipitating, over the ocean, fair-weather cumulus extending to heights of only about 2 km can produce showers [*Ludlam*, 1980; *Battan and Braham*, 1956]. *Kraus* [1963] found that shallow oceanic clouds over the eastern Pacific frequently precipitate. And precipitation-sized droplets in stratocumulus decks less than 400 m thick are frequently observed [*Brost et al.*, 1982a, b; *Nicholls*, 1984; *Albrecht*, 1989]. Although many studies of stratocumulus and trade-cumulus convection have ignored precipitation effects [e.g., *Lilly*, 1968; *Betts*, 1973; *Albrecht et al.*, 1979; *Betts and Ridgway*, 1989], *Redelsperger and Sommeria* [1982] parameterized precipitation processes in large-eddy simulations of trade-cumulus convection and *Nicholls and Turton* [1986] included drizzle in their mixed-layer model of stratocumulus. Since the production of drizzle in shallow clouds may be related to CCN concentrations [e.g., *Squires*, 1958a, b; *Takahashi*, 1977; *Albrecht*, 1989], it is possible that changes in atmospheric aerosol concentrations due to either natural or man-made processes can alter the energetics of the marine boundary layer and the associated cloudiness. Thus drizzle from shallow marine clouds may be an important factor in the climate system.

In this paper the effects of precipitation on the structure of the undisturbed partly cloudy marine boundary layer and the associated energy and moisture balance are examined in detail using a simple boundary layer model. The model used is a version of the model developed by *Albrecht et al.* [1979] (referred to as A79) that is modified to include precipitation processes. In this scheme, the cloud-to-rainwater conversion is modeled by allowing a fixed fraction of the cloud liquid water to precipitate.

In nature the production of drizzle is closely related to cloud microphysical and turbulence effects [*Nicholls*, 1987]. However, in this paper there is no attempt to determine how the precipitation forms, but rather how precipitation alters

the thermodynamic structure of the boundary layer. The steady state thermodynamic structure and the attendant convective fluxes obtained from the model are compared with the corresponding solutions obtained with no precipitation. In addition, the effects that precipitation processes have on the sensitivity of the model to sea surface temperature, surface wind speed and large-scale subsidence are examined.

2. MODEL FORMULATION

2.1. Model Structure

Since the boundary layer model used in this study is described in A79, features of the model that are unaltered from the original version of the model are only summarized; any differences from the original model are discussed in detail.

The A79 model is a one-dimensional model of the undisturbed fair-weather atmospheric boundary layer. Although the model is one-dimensional, the structure simulated is the structure averaged over an area equivalent to that represented by a grid point in a general circulation model. Furthermore, the application described in this paper is limited to oceanic conditions.

The vertical structure is assumed to be a slab structure consisting of a subcloud and a cloud layer (Figure 1). The cloud layer is capped by an inversion layer that is assumed to be infinitesimally thin. The cloud layer and the subcloud layer are separated by a weak inversion layer, the transition layer, that is also assumed to be infinitesimally thin. The vertical coordinate is $\hat{p} = p_0 - p$, where p is pressure and p_0 is the surface pressure. The dependent variables are mixing ratio q and dry static energy $s = c_p T + gz$ where c_p is the specific heat of air at constant pressure, T is temperature in Kelvins, g is the acceleration due to gravity, and z is height. In the subcloud layer it is assumed that the mixing ratio and the dry static energy do not vary with $\hat{p}$ (height), although this assumption could be relaxed. In the cloud layer these variables are assumed to vary linearly. As shown in Figure 1, the layer-averaged values of s and q are represented as s_M and q_M in the subcloud layer and s_A and q_A in the cloud layer. The slopes of these quantities in the cloud layer are γ_s and γ_q. The transition layer is at $\hat{p}_B$, and the inversion at the top of the cloud layer is at $\hat{p}_I$. Since the profiles above the boundary layer are assumed to be either
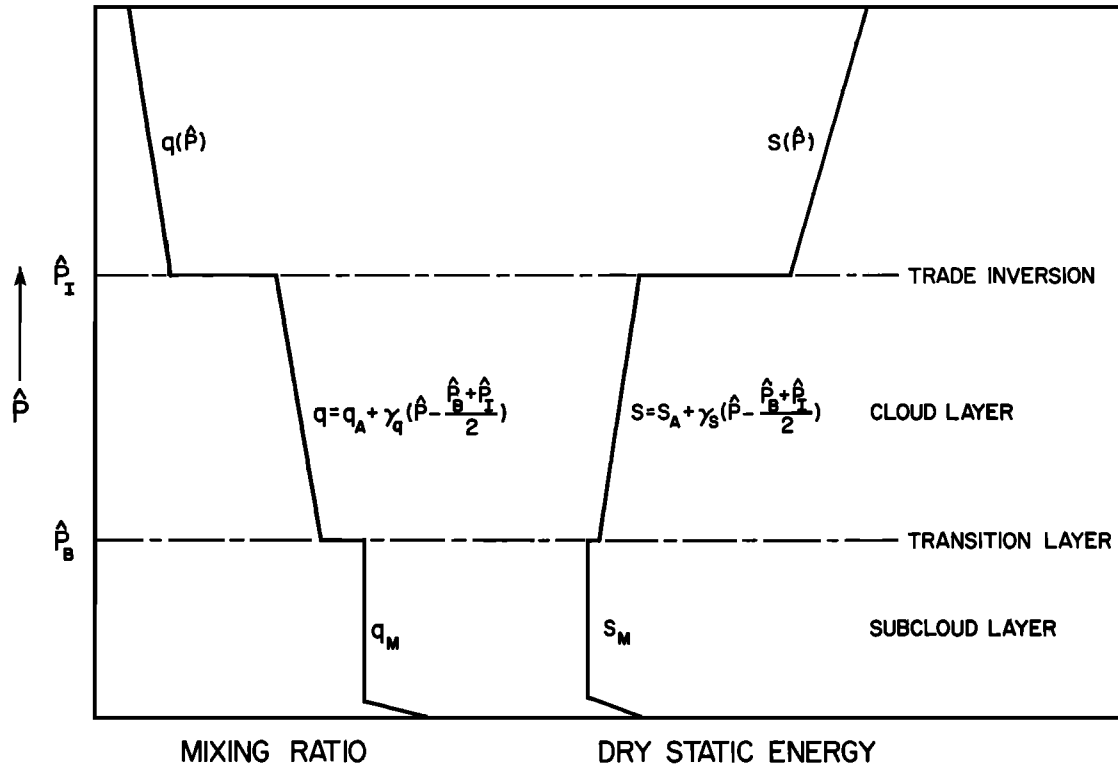
Fig. 1.   Idealized boundary layer structure used in the model.

specified or represented by a large-scale model, the boundary layer structure is predicted by the eight parameters s_M, q_M, s_A, q_A, γ_s, γ_q, $\hat{p}_B$, and $\hat{p}_I$.

2.2. Budget Equations

The time evolution of the boundary layer structure is represented using time and area-averaged budget equations. The budget equations are applied to the simplified structure assumed in the model. These equations are identical to those in A79 except for the addition of terms involving precipitation and the evaporation of precipitation in the subcloud layer. The predictive equations for the subcloud layer are

$$\frac{ds_M}{dt} = -g[(F_s)_{B-} - (F_s)_0]/\hat{p}_B + Q_{RM} - LE_0 \qquad (1)$$

and

$$\frac{dq_M}{dt} = -g[(F_q)_{B-} - (F_q)_0]/\hat{p}_B + E_0 \qquad (2)$$

The subscript B designates quantities at the level of the transition layer; a plus sign and a minus sign will be used to designate quantities just above and just below the structure discontinuities at the base and the top of the cloud layer. F_s is the dry static energy flux, F_q is the water vapor mixing ratio flux, and Q_{RM} is the radiative heating rate averaged over the depth of the subcloud layer. The rate that precipitation is evaporated in the subcloud layer is represented as E_0. Since the subcloud layer is assumed to be well mixed, the mixed layer dry static energy budget is maintained by convective (including evaporative) and radiative processes. The subcloud layer water vapor budget is maintained solely

by convective processes. The total derivatives used in the formulation of (1) and (2) and in the equations given below include only the horizontal derivatives and the local time derivative.

The time variation of the cloud layer-averaged dry static energy and mixing ratio used in A79 are

$$\frac{ds_A}{dt} = \gamma_s\left[\frac{dp_A}{dt} - \hat{\omega}_A\right] - g[(F_{sl})_{I-} - (F_{sl})_{B+}]/\delta\hat{p}$$

$$+ LR_A + Q_{RA} \qquad (3)$$

$$\frac{dq_A}{dt} = \gamma_q\left[\frac{d\hat{p}_A}{dt} - \hat{\omega}_A\right] - g[(F_{q+l})_{I-}$$

$$- (F_{q+l})_{B+}]/\delta\hat{p} - R_A \qquad (4)$$

where the subscript A designates the average value for the cloud layer and the subscript I designates the level of the cloud top inversion. The quantity $\delta\hat{p}$ is the pressure depth of the cloud layer so that $\delta\hat{p} \equiv \hat{p}_I - \hat{p}_B$. The first term on the right side of (3) and (4) relates variations of the cloud-averaged variables to time variations of the mean pressure level of the cloud layer and vertical velocity. For steady state conditions this term reduces to the vertical advection terms. The term $d\hat{p}_A/dt$ may be expressed as a function of the fluxes, using the predictive equations for $\hat{p}_B$ and $\hat{p}_I$ that are given later in this section. The second term on the right side of (3) represents the divergence of the convective flux of the quantity $s - Ll$, where L is the latent heat of vaporization and l is the liquid water mixing ratio. The equivalent term in (4) is the divergence of the convective flux of total water (liquid plus vapor) $q + l$. The R_A term in (3) and (4)

represents the rate of production of precipitation averaged over the depth of the cloud layer. This term is a source term in the heat budget but a sink term in the water vapor budget.

The time variation of the slope of s and q in the cloud layer can be written as

$$\frac{d\gamma_s}{dt} = D_A\gamma_s - 4g[(F_{sl})_{I-} - 2(F_{sl})_A + (F_{sl})_{B+}]/\delta\hat{p}^2$$
$$+ L\left[\frac{\partial R}{\partial \hat{p}}\right]_A + \left[\frac{\partial Q_R}{\partial \hat{p}}\right]_A \quad (5)$$

$$\frac{d\gamma_q}{dt} = D_A\gamma_q - 4g[(F_{q+l})_{I-} - 2(F_{q+l})_A$$
$$+ (F_{q+l})_{B+}]/\delta\hat{p}^2 - L\left[\frac{\partial R}{\partial p}\right]_A \quad (6)$$

where D_A is the large-scale divergence averaged over the depth of the cloud layer, and $(\partial R/\partial \hat{p})_A$ is the layer-averaged vertical derivative of the rainfall rate. The terms involving the flux terms in (5) and (6) are a measure of the curvature of the convective fluxes, and exactly cancel if the fluxes vary linearly with height.

The time variation of the transition layer pressure height and the inversion layer pressure height are

$$\frac{d\hat{p}_B}{dt} = -\hat{\omega}_B + g[(F_{sl})_{B+} - (F_s)_{B-}]/(\Delta s)_B \quad (7)$$

$$\frac{d\hat{p}_I}{dt} = -\hat{\omega}_I - g\frac{(F_{sl})_I - \Delta F_R}{(\Delta s)_I} \quad (8)$$

where no discontinuity in the radiative flux at the transition layer is considered. The large-scale subsidence at $\hat{p}_B$ and $\hat{p}_I$ is $\hat{\omega}_B$ and $\hat{\omega}_I$. Radiative effects at the inversion due to cloud top cooling are parameterized as a radiative flux discontinuity ΔF_R across the inversion and $(\Delta s)_B = s(\hat{p}_{B+}) - s(\hat{p}_{B-})$, $(\Delta s)_I = s(\hat{p}_{I+}) - s(\hat{p}_{I-})$, etc. Equations (7) and (8) are used to eliminate the $d\hat{p}_A/dt$ term from (3) and (4) since $dp_A/dt = (d\hat{p}_B/dt + d\hat{p}_I/dt)/2$.

2.3. Subcloud Convective Fluxes

To solve (1)–(8), it is necessary to represent the various convective and radiative terms as a function of the model structure. In the subcloud layer, dry convective processes are parameterized using the mixed layer closure described by *Betts* [1973], *Tennekes* [1973], and others. In this parameterization, the virtual heat flux at the top of the mixed layer (at $\hat{p}_{B-}$) is assumed to be some negative fraction of the surface flux of virtual dry static energy, where the virtual dry static flux is defined as $F_{sv} = F_s + \delta T_R F_q$, where $\delta = 0.608$, and T_R is a reference temperature. Thus

$$(F_{sv})_{B-} = -k(F_{sv})_o \quad (9)$$

where k is assumed here to have a value of 0.2, although various values have been determined from laboratory and atmospheric measurements [*Stull*, 1976]. The turbulence measurements of *LeMone and Pennell* [1976] support the validity of (9) for the subcloud layer associated with a field of trade cumuli.

The surface fluxes of q and s are parameterized using the bulk aerodynamic formulations

$$(F_s)_o = \rho V C_T(s_o - s_M) \quad (10)$$

$$(F_q)_o = \rho V C_q(q_o - q_M) \quad (11)$$

where s_o is the surface dry static energy and q_o is the saturation mixing ratio of air at the sea surface with a temperature T_o. The bulk transfer coefficients C_T and C_q are assumed to be slightly less than the equivalent coefficients defined at 10 m, since mixed layer values, not 10 m height values, are used in (10) and (11). Here it is assumed that $C_T = C_q = 1.15 \times 10^{-3}$. The surface wind speed V is specified externally for the sensitivity tests shown in this paper.

As described in A79, it can be shown that

$$\frac{(F_q)_{B-}}{(\Delta q)_B} = \frac{(F_s)_{B-}}{(\Delta s)} = \frac{(F_{sv})_{B-}}{(\Delta s_v)_B} \quad (12)$$

Thus, (12) defines the turbulent fluxes just below the transition layer since $(F_{sv})_{B-}$ is defined by (9) as a function of the surface fluxes (see A79 and *Albrecht* [1984]).

2.4. Cloud Layer Convective Fluxes

A cumulus parameterization is used to express the cloud layer convective fluxes and the precipitation terms in (3)–(8) as a function of the large-scale resolvable structure of the boundary layer. Since in A79 precipitation effects were not included, the R and E_0 terms did not appear in the budget equations.

The basic formulation of the convective fluxes follows that of A79 by representing the fluxes as a product of a cumulus mass flux and cloud environment differences. Thus the flux of $s - Ll$ is written as

$$F_{sl} = \frac{\omega^*}{g}[s_c - Ll_c - \bar{s}] \quad (13)$$

where ω^* is the convective mass flux, c designates cloud values, and $\bar{s}$ is the area-averaged dry static energy in the cloud layer and is represented as a function of s_A and γ_s. The equivalent flux for $q + l$ is

$$F_{q+l} = \frac{\omega^*}{g}[q_c + l_c - \bar{q}] \quad (14)$$

Since the cloud layer variables are assumed to have a linear variation with $\hat{p}$, the fluxes are assumed to be quadratic. This quadratic variation is obtained by requiring both ω^* and the cloud environment differences to be linear with $\hat{p}$.

The cloud values that appear in (13) and (14) are obtained by using simple entrainment relationships that were modified to include precipitation effects. For the average cloud, the precipitation at a certain level is assumed to be proportional to the product of the average cloud updraft velocity of active elements and the cloud liquid water content. Since active clouds occupy some fractional area of the domain, the precipitation term in (3)–(6) is represented as

$$R = \omega^* C_o l_c \quad (15)$$

where C_o represents the conversion per pressure interval of cloud water to rain water. The C_o coefficient is a measure of the efficiency of the clouds in converting cloud water to precipitation.

A simple precipitation parameterization like the one used here was tested in a one-dimensional model described by *Simpson and Wiggert* [1969]. This conversion process is also used by *Arakawa and Schubert* [1974] and subsequently by *Albrecht* [1983] in their parameterizations. In the stratocumulus model of *Turton and Nicholls* [1987], the drizzle flux was represented as a function of the integrated water path and the mean droplet radius. This is similar to the parameterization used here since the drizzle flux would be proportional to the integral of $R = C_o \omega^* l_c$. If C_o is assumed to depend on the droplet radius, the parameterization would have a functional form similar to that of *Turton and Nicholls* [1987]. In the parameterization used here, however, the precipitation rate depends on the mass flux, which is proportional to the fractional area occupied with cloud updraft velocity.

The parameter C_o determines how efficiently water is removed from the cloud layer by precipitation processes. As noted previously, its exact specification will depend on cloud microphysical processes that will depend on cloud condensation nuclei (CCN) concentrations. In general, one would expect C_o to be relatively small for continental clouds and large for marine clouds. *Turton and Nicholls* [1987], for example, make their drizzle rate proportional to the mean droplet radius for droplets smaller than 10 μm. Although in some applications a detailed description of the interaction of cloud microphysics and precipitation production would be needed, the focus of this paper is on the effect of the precipitation efficiency on the structure of the convective boundary layer and the physical processes that maintain that structure. Although the majority of the results shown here are determined with no subcloud layer evaporation, simulations were made to determine the effect of evaporation on the subcloud layer thermodynamic structure. These simulations and the specification of B_o are described in section 3. Here we assume a value of $C_o = 10^{-4}$ Pa^{-1} = 1/100 mbar, which is in the range of values suggested by *Betts* [1982].

With the inclusion of precipitation the entrainment equation for $s_c - L l_c$ as given by *Albrecht* [1983] is written

$$\frac{d(s_c - L l_c)}{d\hat{p}} = -E[s_c - L l_c - \bar{s}] + LC_0 l_c \qquad (16)$$

where C_o is the cloud to rainwater conversion factor defined in (15) and E is an entrainment factor. Both of these factors have units of inverse pressure. The corresponding equation describing the vertical variation of total cloud water is

$$\frac{d(q_c + l_c)}{d\hat{p}} = -E[q_c + l_c - \bar{q}] - C_0 l_c \qquad (17)$$

The differential equations (16) and (17) are solved analytically since $\bar{s}$ and $\bar{q}$ are assumed to be linear functions of $\hat{p}$ in the cloud layer. For these solutions the boundary conditions at the cloud base are obtained by assuming that clouds have mixed layer properties and that the cloud base liquid water is zero. With these conditions, $(s_c - L l_c - \bar{s})$ at $\hat{p}_B$ is $-(\Delta s)_B$ and $(q_c + l_c - \bar{q})$ is $-(\Delta q)_B$. The exact solutions to (16) and (17) are exponential and given in the appendix. These solutions are linearized so that

$$[s_c - L l_c - \bar{s}] = -(\Delta s)_B[1 + \lambda_s p'] \qquad (18)$$

and

$$[q_c + l_c - \bar{q}] = -(\Delta q)_B[1 + \lambda_q p'] \qquad (19)$$

where $p' = \hat{p} - \hat{p}_B$. The coefficients λ_s and λ_q in these equations are obtained by assuming that the linear functions of $(s_c - L l_c - \bar{s})$ and $(q_c + l_c - \bar{q})$ given by (18) and (19) when averaged over the depth of the cloud layer and are equal to the average obtained using the exact solutions. The expressions for λ_s and λ_q are given in the appendix and are functions of E, C_o, and the large-scale structure.

The entrainment equations are also used to obtain the cloud liquid water as a linear function of $\hat{p}$ so that

$$l_c = \gamma_l p' \qquad (20)$$

where the slope γ_l is specified so that the average of (20) over the depth of the cloud layer is equal to the average of the exact expression for liquid water (as given in the appendix).

The entrainment parameter E is obtained by applying the constraint

$$\frac{1}{c_p} \int_{\hat{p}_I}^{\hat{p}_B} (s_{vc} - \bar{s}_v)\, d\hat{p} = \alpha$$

$$\cdot \left[\frac{1}{c_p} \int_{\hat{p}_I}^{\hat{p}_B} (s_{vc} - \bar{s}_v)\, d\hat{p} \right]_{max} \equiv b\Delta T_o \delta\hat{p} \qquad (21)$$

where the integral on the right side (and thus ΔT_o) is obtained by assuming that the entrainment parameter E is zero. The equation that results from (21) is given in the appendix. The value of b is unknown, but is bounded as $0 \leq b \leq 1$. Here we assume $b = 0.5$. As b increases, the model entrainment rate will increase. Since (20) is nonlinear, it must be solved numerically. No difficulty with convergence was encountered in any of the solutions obtained in this study. For typical simulations, E has a value of approximately 1/(150 mbar), which is roughly the same magnitude as the value of C_o that has been specified.

To obtain the cloud layer fluxes it is necessary to obtain the cumulus mass flux. The mass flux needed in (13) and (14) is assumed to be a linear function of $\hat{p}$ and goes to zero above the trade inversion so that

$$\omega^* = \omega^*_B(1 + \mu p') \qquad p' \leq \delta\hat{p}$$
$$\omega^* = 0 \qquad p' > \delta\hat{p} \qquad (22)$$

where ω^*_B is the cloud base mass flux. The parameter μ is defined as in A79 and is written as

$$\mu = E - \frac{1}{\omega^*_B \tau_{adj}}(1 + \tfrac{2}{3}E\delta\hat{p}) \qquad (23)$$

where τ_{adj} is a specified time constant that is equivalent to the ratio of individual cloud lifetime to the fractional area covered by active updrafts. A value of one third of a day is assumed for τ_{adj}. Equation (23) was derived using a simple cloud lifetime model similar to that discussed by *Betts* [1975] and is described in A79. The decrease of mass flux with height due to the term is associated with cloud lifetime

effects. *Fraederich* [1973] and *Cho* [1977] also discussed the importance of cloud lifetime effects. The first term on the right-hand side of (23) represents the increase in mass flux with height due to entrainment. Steady state solutions obtained with the A79 model were found to be relatively insensitive to the specification of τ_{adj}. The behavior of the steady state solutions and their sensitivity to τ_{adj} was studied analytically by *Bretherton* [1993].

The cloud base mass flux ω_B^* in (22) is obtained by assuming that the lifting condensation level (LCL) and the transition layer height coincide. This constraint is consistent with observations made during the Global Atlantic Tropical Experiment [*Fitzjarrald and Garstang*, 1981] and following *Betts* [1973] allows one to write

$$\omega_B^* = \hat{\omega}_B - \frac{d\hat{p}_{LCL}}{dt} + \frac{gk(F_{sv})_o}{(\Delta s_v)_B} \qquad (24)$$

where $\hat{p}_{LCL}$ is the $\hat{p}$ at the lifting condensation level of air with mixed layer properties and $(\Delta s_v)_B = s_v(\hat{p}_{B+}) - s_v(\hat{p}_{B-})$. The $\hat{p}_{LCL}$ term in (24) may be represented as a function of the mixed layer fluxes using (1) and (2).

The cloud base mass flux is a critical component of the parameterization. Equation (24) has a straightforward physical interpretation that follows the arguments by *Betts* [1973] and the qualitative discussion given by *Stull* [1985]. The inversion at the cloud base, $(\Delta s_v)_B$, may be viewed as a valve that regulates the exchange of mass between the subcloud and the cloud layer. Eddies in the subcloud layer will have a range of vertical velocities. Thus only those eddies of sufficient kinetic energy will penetrate the transition layer inversion, and some of these may become clouds if their LCL is sufficiently low. The release of latent heat in eddies that reach their LCL provides additional energy that can be used to overcome an area of negative buoyancy that exists just above the cloud base.

The effect of the large-scale vertical velocity on the cloud base mass flux is also illustrated by (24). If all other factors are held fixed and the subsidence at cloud base decreases, the tendency would be for the height of the transition layer to increase. Since the mean mixed layer values are not directly affected by the mean subsidence, the LCL is unchanged but would now be below the height of the transition layer. Consequently, more subcloud layer convective elements will reach their LCL and thus enhance the cloud base mass flux, which would subsequently decrease the transition layer height. If subcloud layer processes lower the mean LCL (assuming all other factors including the transition layer height remain fixed), more eddies would reach their LCL and the cloud base mass flux would increase, and this would lower the transition layer height to the height of the LCL. This behavior is clearly consistent with (24). If the surface heat flux (which provides energy to the subcloud layer eddies) increases, more subcloud layer eddies would reach their LCL and the cloud base mass flux would increase. Similarly, if the transition layer inversion decreases in strength $((\Delta s_v)_B$ decreases), the cloud base mass flux would increase since more subcloud eddies would be able to reach their LCL, a behavior that is again consistent with (24).

2.5. Radiative Fluxes

The radiative heating rates in (1), (3), and (5) and the radiative flux divergence term in (8) are specified following

TABLE 1. Closure Parameters and Physical Parameters Specified Externally in the Model

Parameter	Value
Closure Parameters	
k	0.20
C_T	1.15×10^{-3}
τ_a	1/3 day
b	0.5
Physical Parameters	
T_o	25°C
V	8 ms^{-1}
D	$5 \times 10^{-6} \text{ s}^{-1}$
s_{oo}	300.0 kJkg^{-1}
q_{oo}	8.0 gkg^{-1}
Γ_s	$4.67 \times 10^{-2} \text{ kJkg}^{-1} \text{ mbar}^{-1}$
Γ_q	$1.43 \times 10^{-2} \text{ gkg}^{-1} \text{ mbar}^{-1}$

the simple parameterization described in A79. That parameterization was based on calculations that show the radiative cooling averaged over the depth of the boundary layer to be independent of the depth of the boundary layer, the moisture content of the boundary layer and the amount of cloudiness. The vertical distribution, however, depends on cloud amount. Here we choose a very simple distribution where some fraction of the clouds penetrate into the inversion and contribute to radiative cooling at the inversion due to cloud top cooling. This cooling equates to a flux divergence in (5) and depends on a specified cloud amount. Below the inversion the cooling is distributed uniformly over the depth of the cloud layer. For the simulations shown here, a fractional cloudiness of 0.25 is assumed, with a cooling rate through the depth of the boundary layer of 3°C/day, consistent with the value used in A79. This specification gives $Q_{RM}/c_p = Q_{RA}/c_p = -2.25°C$, $(\partial Q_R/\partial \hat{p}) = 0$ and $\Delta F_R = \hat{p}_I Q_I/g$ where $Q_I/c_p = -0.75°C/day$. For the studies here, the feedbacks due to radiative processes are intentionally suppressed to evaluate the impact of drizzle on the boundary layer structure.

The predicative (1)–(8) represent eight equations for the eight unknowns needed to describe the thermodynamic structure of the boundary layer. The flux $(F_{q+l})_{I-}$ given by (14) is adjusted slightly as described in A79 to ensure that the temperature and moisture discontinuities are maintained at the same level $\hat{p}_I$. Without this adjustment the model will not exactly conserve moisture.

With the parameterizations described above, the model equations can be solved numerically provided the profiles of s and q above the inversion, surface wind speed, large-scale divergence, and sea surface temperature are specified. The thermodynamic structure above the inversion is specified as a linear function of $\hat{p}$ as $s(\hat{p}) = s_{oo} + \Gamma_s \hat{p}$ and $q(\hat{p}) = q_{oo} + \Gamma_q \hat{p}$ where the coefficients used in these expressions are those used in *Albrecht* [1984] and are consistent with the profiles observed during the Atlantic Trade-Wind Experiment (ATEX) in 1969. The various coefficients needed for the closures in the model are those specified by *Albrecht et al.* [1979] and *Albrecht* [1984], and are summarized in Table 1. The equations are solved using a fourth-order Runge-Kutta scheme with a time step of 500 s.

3. STEADY STATE SOLUTIONS

Steady state solutions from the numerical integration of the model are used to show how the thermodynamic struc-
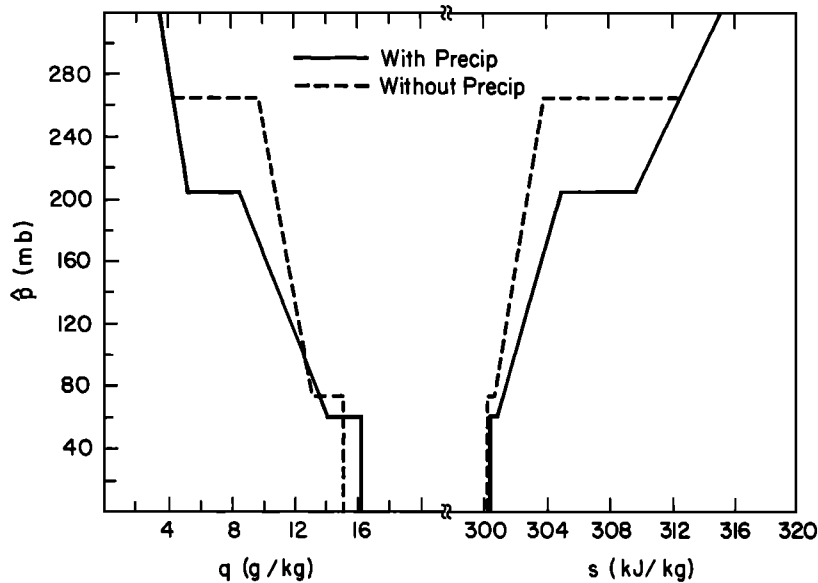
Fig. 2. Steady state mixing ratio and dry static energy obtained with and without precipitation.

ture is maintained by large-scale, convective, and radiative processes. A comparison of the thermodynamic structure obtained with and without precipitation is shown in Figure 2 and the convective fluxes corresponding to these solutions are shown in Figure 3. The simulation with precipitation is made with no evaporation of rain in the subcloud layer and with C_o = 1/100 mbar. The case with precipitation is designated as case P; the case without precipitation is designated as case NP. The external parameters used for these solutions are shown in Table 1.

Although the precipitation rate for case P is only about 0.8 mm/day, the removal of water at this rate has a substantial impact on the thermodynamic structure predicted with the model. In the cases shown here, the inclusion of precipitation lowers the inversion height by about 50 mbar, weakens

the inversion by about 4 K, dries and warms the cloud layer, and increases the cloud layer stratification.

The inversion height is decreased since precipitation depletes the cloud water available for evaporation at cloud top. As the cooling and moistening is decreased, the warming and drying due to the large-scale subsidence lowers the inversion. As the inversion is lowered, the large-scale subsidence decreases (divergence is constant), and a new balance is established at a lower level. This is shown in Table 2 where the tendencies on the right-hand side of the equation that predicts the inversion height (see equation (8)) are compared for both the nonprecipitating and precipitating cases. The rate at which the inversion height is increased by convective processes is halved when precipitation is included.

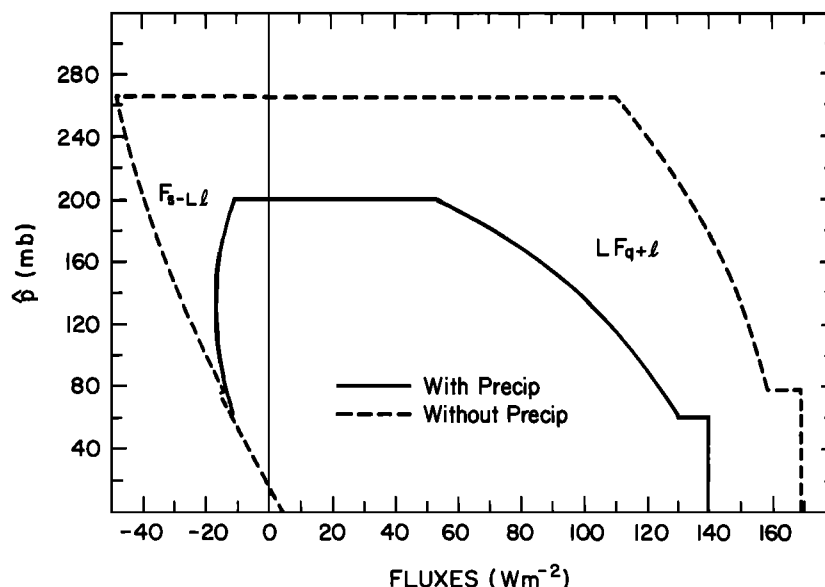For the steady state solutions, the tendencies due to

Fig. 3. Fluxes associated with the steady state solutions shown in Figure 2.

vertical velocity, convective flux divergence, and the radiative flux divergence balance. The magnitude of F_{s-Ll} at cloud top decreases by approximately 38 Wm^{-2} due to the removal of liquid water l. Since the strength of the inversion decreases, the tendency due to the radiative effects, which is proportional to the radiative flux divergence divided by the strength of the inversion, increases and dominates over the convective flux divergence term when precipitation is included.

The relative drying and warming of the cloud layer for the P and NP cases are illustrated by the tendencies listed in Table 3. In the nonprecipitating case, the warming due to large-scale subsidence and the convergence of the flux of F_{s-Ll} balance the radiative cooling. With precipitation, however, the radiative cooling is balanced by the latent heating due to precipitation and the heating due to the large-scale subsidence with little net contribution by the convective flux divergence. The subsidence warming increases because of the increased stability in the cloud layer. The drying subsidence of the cloud layer is simply balanced by the flux convergence of the total water for the case with no precipitation. With precipitation, the removal of water by precipitation results in a decrease of the moisture flux with height, as shown in Figure 3. This results in the increased moistening that balances the drying due to precipitation and the increased drying due to the large-scale subsidence (Table 3) as the stratification increases.

The inclusion of precipitation has a substantial impact on the stratification in the cloud layer. In the solutions presented here, radiation is not allowed to alter the slope of s. Thus for the equilibrium solutions in the nonprecipitating case, the stabilizing effect of the large-scale subsidence is balanced by the destabilization due to the convective fluxes. This destabilization is due to the quadratic variation with height of F_{sl}. In the precipitation case the curvature of the flux increases, and as shown in Figure 3, this increased destabilization is needed to balance the stabilization due to both the subsidence and precipitation (see Table 4).

Precipitation also alters the slope of q in the cloud layer. In the precipitating case the vertical velocity and the precipitation act to increase the slope of q, while convective fluxes (as indicated by the increased curvature shown in Figure 3) tend to decrease the slope.

The difference in the subcloud layer temperature between the precipitating and the nonprecipitating cases is small. The subcloud layer mixing ratio is, however, about 1 g/kg higher in case P than in case NP. Thus the surface flux of latent heat decreases from 170 Wm^{-2} for the nonprecipitating case to 140 Wm^{-2} for the precipitating case. Steady state solutions require this reduction in the surface moisture flux since the total drying by the large-scale subsidence is reduced as the overall depth of the boundary layer is reduced when precipitation is included. The subsidence drying is balanced by the

TABLE 3. Tendency Terms in the Cloud Layer Budgets of Mean s (See Equation (3)) and q (See Equation (4))

Process	$\frac{1}{c_p}\frac{\partial s_A}{\partial t}$, °C day^{-1}		$\frac{\partial q_A}{\partial t}$, g kg^{-1} day^{-1}	
	NP	P	NP	P
Large-Scale	0.73	0.99	−0.83	−1.29
Convection	1.52	−0.06	0.87	1.83
Precipitation	···	1.32	···	−0.54
Radiation	−2.25	−2.25	···	···

convergence of the surface moisture flux over the depth of the boundary layer.

The steady state solutions obtained with evaporation of precipitation in the subcloud layer differ little from those with no evaporation. Evaporation was included by assuming that the evaporation rate depends on the relative humidity in the subcloud layer so that in (1) and (2) is represented as $E = B_o \hat{p}_B (1 - RH_M)R_A$ where RH_M is the subcloud layer relative humidity, R_A is the rate that precipitation is generated in the cloud layer and B_o defines how efficiently the rain will be evaporated. Although this efficiency will principally depend on the size of the droplets [Pruppacher and Klett, 1978], B_o in the solution described here is specified as a constant of 2×10^{-4} Pa^{-1}. This corresponds to a pressure scale for evaporation of 50 mbar, which is within the range of 30–100 mbars suggested by Betts [1982].

With evaporation, the precipitation reaching the surface is reduced from 0.8 mm/day to 0.6 mm/day. The precipitation generated in the cloud layer, however, increases slightly to about 0.9 mm/day so that approximately 0.3 mm/day is evaporated in the subcloud layer. Despite the evaporation, the solutions differ little from the case discussed previously where no evaporation is permitted. The subcloud layer is cooled by approximately 0.3°C and moistened by about 0.2 g/kg, which results in a slight increase in the subcloud relative humidity. The inversion in the case with evaporation is approximately 2 mbar lower than the case with no evaporation. There are, however, substantial changes in the moisture and heat budgets of the subcloud layer as indicated by the subcloud layer tendencies summarized in Table 5. The evaporation substantially cools and moistens the subcloud layer. This moistening and cooling, however, is balanced by an increased divergence of the moisture fluxes. Furthermore, although the evaporation of drizzle in the subcloud has little effect on the equilibrium structure, it may play a critical role in the initial formation of the stable layer at cloud base.

4. SENSITIVITY TESTS

Simulations were made to determine the sensitivity of the model to the specification of the precipitation efficiency. The precipitation rates from the model are sensitive to the specification of C_o at low values of C_o as shown in Figure 4. However, for higher C_o values, both the precipitation rates and the thermodynamic structure are relatively insensitive to the specification of C_o. For $C_o = 0.0001$ Pa^{-1} the liquid water content in the parameterized clouds near the inversion is 1.1 g/kg. For the case with $C_o = 0$, the cloud liquid water content is 2.8 g/kg.

TABLE 2. Tendency Terms in the Inversion Height Budget (See Equation (8)) for Steady State Conditions

Process	No Precipitation, NP	Precipitation, P
Large-Scale	−68.8	−53.2
Convection	47.5	19.9
Radiation	21.3	33.3

Units are in millibars per day.

TABLE 4. Tendency Terms in the Cloud-Layer Budgets of γ_s (See Equation (5)) and γ_q (See Equation (6))

Process	$\dfrac{\partial \gamma_s}{\partial t}$, J kg^{-1} Pa^{-1} day^{-1}		$\dfrac{\partial \gamma_a}{\partial t}$, g kg^{-1} kPa^{-1} day^{-1}	
	NP	P	NP	P
Large-Scale	0.042	0.068	−0.049	−0.097
Convection	−0.042	−0.151	0.049	0.136
Precipitation	⋯	0.083	⋯	−0.039

Model simulations were made to determine the sensitivity of precipitation rates to the specification of sea surface temperature, radiative cooling, large-scale divergence, and surface wind speed. For these simulations $C_o = 1.0 \times 10^{-4}$ Pa^{-1}. With a divergence of 5×10^{-6} s^{-1}, the precipitation rate increases from near zero at 22°C to 0.6 mm/day at 30°C (Figure 5). The precipitation rates however, are very sensitive to the specification of divergence. When the divergence is reduced from 5×10^{-6} s^{-1} to 3×10^{-6} s^{-1}, the precipitation rate at 30°C is more than tripled.

The combined sensitivity of the precipitation rates to sea surface temperature and large-scale divergence may partially explain why inversion heights observed over the equatorial Pacific average between 850–800 mbar, with remarkably little variability [Kloesel and Albrecht, 1989]. As the boundary layer deepens downstream due to increasing temperature and decreasing divergence, increased precipitation acts to diminish the growth rate of the inversion height relative to the case where no precipitation is included. The precipitation rate increases under these conditions and acts to keep the inversion lower than it would be without precipitation. Thus the sensitivity of the height of the inversion to variations in large-scale divergence and sea surface temperature is reduced when precipitation is included.

The precipitation rate is sensitive to wind speed as shown in Figure 6. As the wind speed increases, the evaporation from the surface increases. Without precipitation, this increased evaporation results in a deeper boundary layer. As the boundary layer deepens, the mean drying by subsidence increases and acts to balance the evaporative moistening. As discussed previously, when precipitation is included, any deepening of the boundary layer increases the precipitation rate, which depletes the liquid water and allows the inversion to be maintained at a lower level with less subsidence drying than would exist without the drizzle.

The precipitation rate is relatively sensitive to the radiative heating averaged over the depth of the boundary layer as

shown in Figure 7. As the cooling is increased, the precipitation rate increases. Although diurnal calculations were not made with the model, the steady state results suggest that the drizzle might be reduced during the day when solar heating in the cloud layer would balance some of the cooling.

The variations of the precipitation rates due to changes in sea surface temperature, radiative cooling rates, divergence, and surface wind speed are most closely related to the depth of the cloud layer (Figure 8). The increase of precipitation rate with increasing cloud depth is very similar for these sensitivity tests and is approximately 1 mm/day/km. For a fixed precipitation efficiency it may be possible to parameterize the precipitation rates as a function of the cloud depth in simple models. As the precipitation efficiency C_o is varied, however, there is an inverse relationship between cloud depth and of the precipitation rate (see curve PE on Figure 8). Thus processes that alter C_o will complicate the representation of drizzle in simple applications of this model.

5. CONCLUSIONS

A model that represents the thermodynamic structure of the trade wind boundary layer as a simple layered structure was modified to allow for the removal of water by precipitation processes. It was shown that precipitation rates of less than 1 mm/day have a substantial impact on the thermodynamic structure of the boundary layer. Precipitation dries and warms the cloud layer. Since less water is available to evaporate at the top of the cloud layer, the inversion is lower than where there is no precipitation. As sea surface temperature increases and divergence decreases, the precipitation rates increases. This increase in precipitation tends to de-

TABLE 5. Tendency Terms in the Subcloud Layer Budgets of s (Equation (1)) and q (Equation (2)) for the Precipitation Only Case (P) and the Case With Evaporation in the Subcloud Layer (PE)
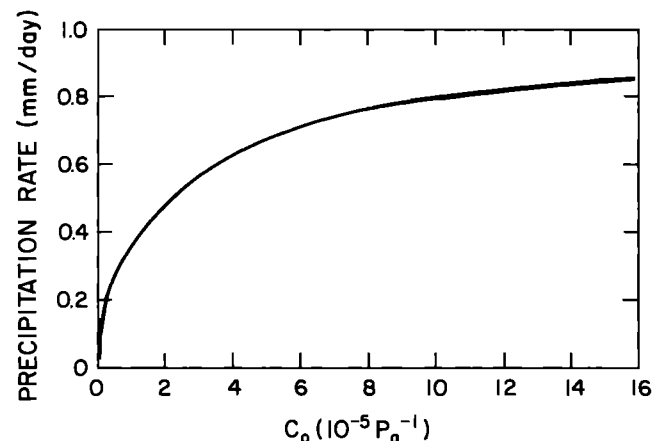
Process	$\dfrac{1}{c_P}\dfrac{\partial s_M}{\partial t}$, °C day^{-1}		$\dfrac{\partial q_M}{\partial t}$, g kg^{-1} day^{-1}	
	P	PE	P	PE
Convection	2.25	3.25	⋯	−0.41
Radiation	−2.25	−2.25	⋯	⋯
Evaporation	0	−1.00	⋯	+0.41

Fig. 4. Precipitation rate as a function of specified values of C_o.

crease the sensitivity of the inversion height to wind speed, sea surface temperature, large-scale divergence, and the radiative cooling in the boundary layer.

Low-level inversions play a critical role in inhibiting deep convection in equatorial regions [*Firestone and Albrecht*, 1986; *Kloesel and Albrecht*, 1989]. The undisturbed regions surrounding deep convection have a boundary layer structure that is similar to that found in the subtropics [*Betts and Albrecht*, 1987]. Although the equatorial regions may often experience mean upward motion, the regions surrounding deep convective systems may experience subsidence that is of nearly the same magnitude as that in the subtropics. The inversions over the central and eastern equatorial Pacific are found to have an average height of 800–850 mbar with little variation with latitude or longitude [*Kloesel and Albrecht*, 1989]. These heights are similar to those observed in the subtropics [*Augstein et al.*, 1974; *Riehl et al.*, 1951]. Although the subsidence field may be an important factor in determining the inversion height, the removal of water by precipitation processes may weaken and lower the inversion relative to the nonprecipitation case. Clearly, as the boundary layer and associated cloud layer deepen and moisten along equator-bound trajectories, the potential for precipitation increases. Thus precipitation in shallow cumulus may retard the deepening of the boundary layer as air moves equatorward in the trades. Consequently, precipitation acts to limit the inversion height as temperature increases and the divergence weakens.

A number of pressure scales are fundamental to this model. These scales control lateral entrainment (E^{-1}), precipitation production (C_o^{-1}), evaporation of precipitation (E_o^{-1}), and the cumulus mass flux distribution (μ^{-1}). As described by *Betts* [1992], these scales provide a simplification of complex processes. Studies aimed at better understanding these processes, like those using data recently collected during the Atlantic Stratocumulus Transition Ex-
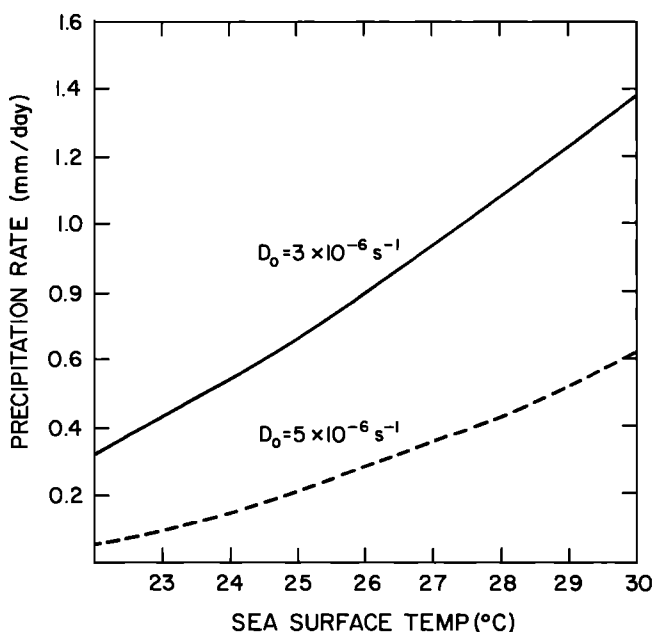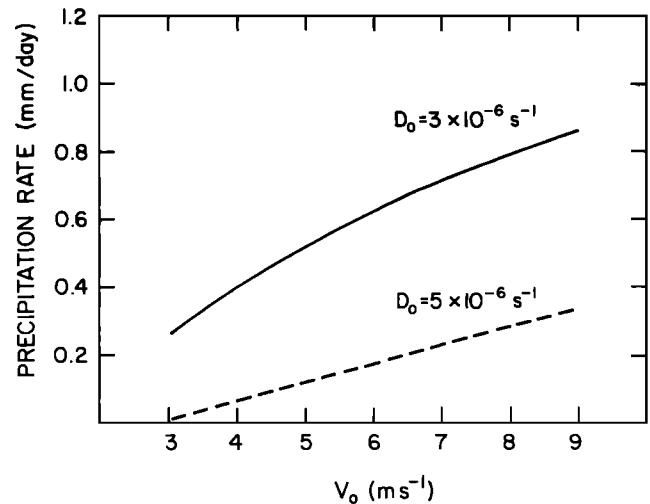

Fig. 6. Precipitation rate as a function of wind surface wind speed for two values of divergence.

periment (in 1992), should lead to improved parameterizations for the model.

The inclusion of precipitation decreases the predicted cloud cover by drying the cloud layer and reducing the liquid water content in the cloud layer as shown by *Albrecht* [1989]. This has important implications for climate modeling. *Wang et al.* [1993] implemented a generalized version of the model described in this paper in a regional model. This model simulates both stratocumulus and trade cumulus and was applied to a region over the eastern Pacific. Cloud cover over this region was decreased by 43% when precipitation effects were included.

Since several simplifications have been made in the model to facilitate the interpretation of the results, further work is needed to improve and evaluate the model before it is implemented a climate model. *Bretherton* [1992], for example, shows that the cloud cover predicted with the A79 model is sensitive to the closure parameters b and τ_{adj}. An interactive radiative scheme would have to be included if this model were to be applied in a climate model or to study the feedbacks between the radiative and the convective

Fig. 5. Precipitation rate as a function of sea surface temperature for two values of specified large-scale divergence.
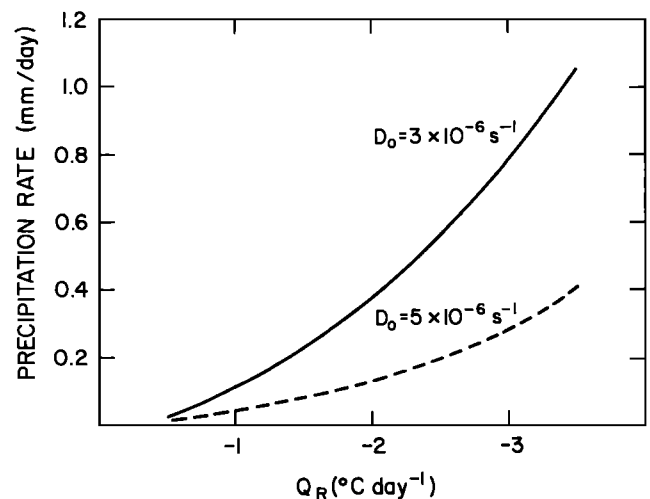

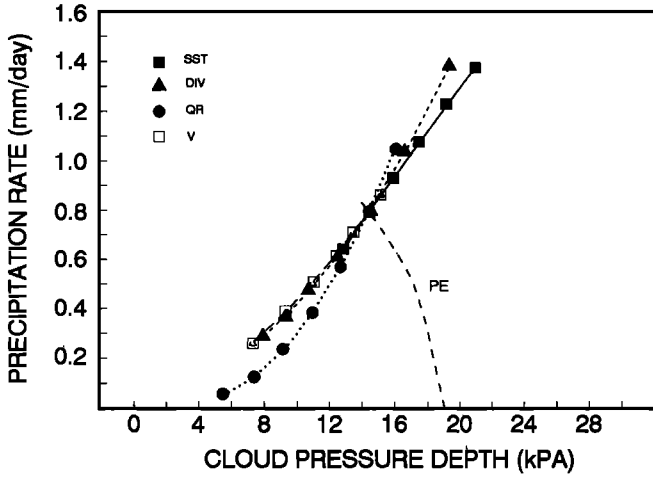Fig. 7. Precipitation rate as a function of radiative heating rate.

Fig. 8. Precipitation rate as a function of cloud depth for sensitivity tests discussed previously. The curve labeled PE is for values of C_o ranging from 0 to $1.5 \times 10^{-1} \mathrm{Pa}^{-1}$.

fluxes. The precipitation scheme used here is very simple and could be modified to link cloud microphysics and precipitation rates to CCN concentrations. In addition, as illustrated by Baker and Charlson [1990], the CCN concentration can be altered by the precipitation process. With appropriate modifications the model could be used to predict not only the thermodynamic structure, but CCN concentrations.

APPENDIX

Solutions of Entrainment Equations

The entrainment equations (16) and (17) can be combined to give $dh_c/d\hat{p} = -\lambda(h_c - \bar{h})$. The analytical solution of this equation is

$$h_c - \bar{h} = -(\Delta h)_{CB} + \left[(\Delta h)_{CB} - \frac{\gamma_n}{E'} \delta\hat{p} \right]$$

$$\cdot \left[1 - \exp\left(-\frac{E'p'}{\delta\hat{p}} \right) \right] \qquad (A1)$$

The analytical solution to (17) is

$$q_c + l_c - \bar{q} = -(\Delta q)_{CB} + \frac{C'_o}{E' + C'_o} [\gamma_{qc} - \dot{\gamma}_q]p' + A(p')$$

$$\cdot \left[\frac{E'(E' + C'_o)(\Delta q)_{CB} - (E'\gamma_q + C'_o\gamma_{qc})\delta\hat{p}}{(E' + C'_o)^2} \right], \qquad (A2)$$

This equation can be rewritten to give

$$l_c = \frac{E'}{E' + C'_o} [\gamma_q - \gamma_{qc}] + A(p')$$

$$\cdot \left[\frac{E'(E' + C'_o)(\Delta q)_{CB} - (E'\gamma_q + C'_o\gamma_{qc})\delta\hat{p}}{(E' + C'_o)^2} \right] \qquad (A3)$$

where $A(p') = \{1 - \exp[-(E' + C'_o)p'/\delta\hat{p}]\}$. Here $E' = E\delta\hat{p}$ and $C'_o = C_o\delta\hat{p}$ are the nondimensional entrainment and liquid water conversion parameters. These equations are used to form linear functions by assuming that the linearized expressions averaged over the depth of the cloud layer are equal to the average of the exact solutions given by (A1)–

(A3). This linearization can be used to give λ_n in $h_c - \bar{h} = -(\Delta h)_B(1 + \lambda_n p')$, λq in (19) and γ_l in (20) as

$$\lambda_h = [\gamma_h/(\Delta h)_{CB} - E'/\delta\hat{p}](\exp(-E') - 1 + E')/E^{2'}, \qquad (A4)$$

$$\lambda_q = -\frac{C'_o}{(\Delta q)_{CB}(E' + C'_o)} (\gamma_{qc} - \gamma_q) - 2B/(\Delta q)_{CB}, \qquad (A5)$$

and

$$\gamma_l = \frac{E'}{E' + C'_o} (\gamma_q - \gamma_{qc}) + 2B \qquad (A6)$$

where

$$B = \frac{E'(E' + C'_o)(\Delta q)_{CB} - (E'\gamma_q + C'_o\gamma_{qc})\delta\hat{p}}{\delta\hat{p}(E' + C'_o)^3}$$

$$\cdot [(\exp[-E' + C'_o)] + (E' + C'_o) - 1)].$$

For a given value of E', λ_h can be calculated using (A4). The slope of q in the cloud can then be calculated by noting that

$$q_c - \bar{q^*} = \frac{\gamma}{1 + \gamma} \frac{1}{L} [h_c - \bar{h^*}] \qquad (A7)$$

so that

$$\gamma_{qc} = \gamma_q^* + \frac{\gamma}{1 + \gamma} \frac{1}{L} [\gamma_h - (\Delta h)_{CB}\lambda_h - \gamma_s - L\gamma_q^*] \qquad (A8)$$

since $\gamma_{hc} = \gamma_h - (\Delta h)_{CB}\lambda_h$ and $\gamma_h^* = \gamma_s + L\gamma_q^*$. The quantity γ_{qc} is easily calculated since γ_q^* can be calculated from λ_s and is used in (A5) and (A6) to calculate λ_q and γ_l.

The entrainment parameter E' is obtained by solving (21) numerically. The expression for $s_{vc} - \bar{s_v}$ is derived by Albrecht et al. [1979] and is

$$s_{vc} - s_v = -\beta(\Delta h)_{CB}(1 + \lambda_h p') + \varepsilon L(\Delta q)_{CB}(1 + \lambda_q p')$$

$$- \alpha L[q_B^* - q_{B+} + (\gamma_q^* - \gamma_q)p'], \qquad (A9)$$

where the notation is that defined in A79 and $\varepsilon = 0.12$, $\alpha = 0.31$ and $\beta = 0.50$. When (A9) is substituted into (21), the equation that results is

$$f(E') = 0 = [bc_pT_0 + \beta(\Delta h)_{CB} - \varepsilon L(\Delta q)_{CB}$$

$$+ \alpha L(q_B^* - \bar{q_B})] \frac{2}{\delta\hat{p}} + \alpha L(\gamma_q^* - \gamma_q)$$

$$+ \beta(\Delta h)_{CB}\lambda_h - \varepsilon L(\Delta q)_{CB}\lambda_q \qquad (A10)$$

where λ_h and λ_q are defined by (A4) and (A5) and are the only factors in (A10) that involve E'. The factor ΔT_o is obtained by assuming $E' = 0$. Initial guesses of $E' = 0.05$ and $E' = 2.00$ are used to solve for an E' that satisfies (21). The iteration is made until successive values differ by less than 0.01 (i.e., $|E'_{i+1} - E'_i| < 0.01$).

Precipitation Terms

The change in mixing ratio due to precipitation is

$$\left(\frac{dq}{dt} \right)_{precip} = -\omega_B^*(1 + \mu p')c_o\gamma_l p'/\delta\hat{p} \qquad (A11)$$

and

$$\frac{\partial}{\partial \hat{p}} \left(\frac{dq}{dt} \right)_{precip} = -\omega_B^*(1 + 2\mu p')c_o\gamma_l/\delta\hat{p} \quad\text{(A12)}$$

These equations are averaged over the depth of the cloud layer to give

$$R_A = -\omega_B^* c_o \gamma_l(\tfrac{1}{2} + \tfrac{1}{3}\mu\,\delta\hat{p}) \quad\text{(A13)}$$

and

$$\left(\frac{\partial R}{\partial \hat{p}} \right)_A = -\omega_B^* c_o \gamma_l(1 + \mu\,\delta\hat{p})/\delta\hat{p}. \quad\text{(A14)}$$

REFERENCES

Albrecht, B. A., Parameterization of trade-cumulus cloud amounts, *J. Atmos. Sci.*, *38*, 97–105, 1981.

Albrecht, B. A., A cumulus parameterization for climate studies of the tropical atmosphere, Part I, Model formulation and sensitivity tests, *J. Atmos. Sci.*, *40*, 2166–2182, 1983.

Albrecht, B. A., A model study of downstream variations in the thermodynamic structure of the trade wind, *Tellus*, *36A*, 187–202, 1984.

Albrecht, B. A., Aerosols, cloud microphysics, and fractional cloudiness, *Science*, *245*, 1227–1230, 1989.

Albrecht, B. A., A. K. Betts, W. H. Schubert, and S. K. Cox, A model of the thermodynamic structure of the trade-wind boundary layer, Part I, Theoretical formulation and sensitivity tests, *J. Atmos. Sci.*, *36*, 73–89, 1979.

Arakawa, A., and W. H. Schubert, Interaction of a cumulus cloud ensemble with the large-scale environment, Part I, *J. Atmos. Sci.*, *31*, 674–701, 1974.

Augstein, E., H. Schmidt, and F. Ostapoff, The vertical structure of the atmospheric planetary boundary layer in undisturbed trade winds over the Atlantic Ocean, *Bound. Layer Meteorol.*, *6*, 129–150, 1974.

Baker, M. B., and R. J. Charlson, Bistability of CCN concentrations and thermodynamics in the cloud-topped boundary layer, *Nature*, *345*, 142–144, 1990.

Battan, L. J., and R. R. Braham, Jr., A study of convective precipitation based on cloud and radar observations, *J. Meteorol.*, *13*, 587–591, 1956.

Betts, A. K., Non-precipitating cumulus convection and its parameterization, *Q. J. R. Meteorol. Soc.*, *86*, 178–196, 1973.

Betts, A. K., Parametric interpretation of trade-wind cumulus budget studies, *J. Atmos. Sci.*, *32*, 1934–1945, 1975.

Betts, A. K., Cloud thermodynamic models in saturation point coordinates, *J. Atmos. Sci.*, *39*, 2182–2191, 1982.

Betts, A. K., and B. A. Albrecht, Conserved parameter analysis of the convective boundary layer thermodynamic structure over the tropical oceans, *J. Atmos. Sci.*, *44*, 83–99, 1987.

Betts, A. K., and W. Ridgway, Climatic equilibrium of the atmospheric convective boundary layer over a tropical ocean, *J. Atmos. Sci.*, *46*, 2621–2641, 1989.

Bretherton, C. S., Understanding Albrecht's model of trade cumulus cloud fields, *J. Atmos. Sci.*, in press, 1993.

Brost, R. A., D. H. Lenschow, and J. C. Wyngaard, Marine stratocumulus layers, Part I, Mean Conditions, *J. Atmos. Sci.*, *39*, 800–817, 1982a.

Brost, R. A., D. H. Lenschow, and J. C. Wyngaard, Marine stratocumulus layers, Part II, Turbulence budgets, *J. Atmos. Sci.*, *39*, 818–836, 1982b.

Cho, H.-R., Contribution of cumulus life-cycle effects to the large-scale heat and moisture budgets, *J. Atmos. Sci.*, *34*, 87–97, 1977.

Firestone, J., and B. A. Albrecht, The structure of the atmospheric boundary layer in the central equatorial Pacific during FGGE, *Mon. Weather Rev.*, *114*, 2219–2231, 1986.

Fitzjarrald, D. R., and M. Garstang, Vertical structure of the tropical boundary layer, *Mon. Weather Rev.*, *10*, 1512–1526, 1981.

Fraedrich, K., On the parameterization of cumulus convection by lateral mixing and compensating subsidence, *J. Atmos. Sci.*, *30*, 408–413, 1973.

Kloesel, K. A., and B. A. Albrecht, Low-level inversions over the tropical Pacific—Thermodynamic structure of the boundary layer and the above-inversion moisture structure, *Mon. Weather Rev.*, *117*, 87–101, 1989.

Kraus, E. B., The diurnal precipitation change over the sea, *J. Atmos. Sci.*, *20*, 551–556, 1963.

LeMone, M. A., and W. T. Pennell, The relationship of trade wind cumulus distribution to subcloud layer fluxes and structure, *Mon. Weather Rev.*, *104*, 524–539, 1976.

Lilly, D. K., Models of cloud-topped mixed layers, *Q. J. R. Meteorol. Soc.*, *94*, 292–309, 1968.

Ludlam, F. H., *Clouds and Storms*, 405 pp., The Pennsylvania State University Press, University Park, Pa., 1980.

Nicholls, S., The dynamics of stratocumulus: Aircraft observations and comparisons with a mixed layer model, *Q. J. R. Meteorol. Soc.*, *110*, 783–820, 1984.

Nicholls, S., A model of drizzle growth in warm, turbulent, stratiform clouds, *Q. J. R. Meteorol. Soc.*, *113*, 1141–1170, 1987.

Nicholls, S., and J. D. Turton, An observational study of the structure of stratiform cloud sheets: Part I, Structure, *Q. J. R. Meteorol. Soc.*, *112*, 431–460, 1986.

Pruappacher, H. R., and J. D. Klett, *Microphysics of Clouds and Precipitation*, 714 pp., D. Reidel, Norwell, Mass., 1978.

Redelsperger, J. L., and G. Sommeria, Methode de representation de la turbulence associee aux precipitations dans un modele tri-dimensionnel de convection nuageuse, *Bound. Layer Meteorol.*, *24*, 231–252, 1982.

Riehl, H., T. C. Yeh, J. S. Malkus, and N. E. LaSeur, The northeast trade of the Pacific Ocean, *Q. J. R. Meteorol. Soc.*, *77*, 598–626, 1951.

Simpson, J., and V. Wiggert, Models of precipitating cumulus towers, *Mon. Weather Rev.*, *97*, 471–489, 1969.

Squires, P., The microstructure of colloidal stability of warm clouds, Part II, The causes of the variations in microstructure, *Tellus*, *10*, 262–271, 1958a.

Squires, P., Penetrative downdraughts in cumuli, *Tellus*, *10*, 381–389, 1958b.

Stull, R. B., The energetics of entrainment across a density interface, *J. Atmos. Sci.*, *30*, 558–567, 1976.

Stull, R. B., A fair-weather cumulus cloud classification scheme for mixed-layer studies, *J. Clim. Appl. Meteorol.*, *24*, 49–56, 1985.

Takahashi, T., A study of Hawaiian warm rain showers based on aircraft observation, *J. Atmos. Sci.*, *34*, 1773–1790, 1977.

Tennekes, H., A model for the dynamics of the inversion above a convective boundary layer, *J. Atmos. Sci.*, *30*, 558–567, 1973.

Turton, J. D., and S. Nicholls, A study of the diurnal variation of stratocumulus using a multiple mixed layer model, *Q. J. R. Meteorol. Soc.*, *113*, 969–1009, 1987.

Wang, S., B. A. Albrecht, and P. M. Minnis, Regional modeling of marine boundary layer clouds, *J. Atmos. Sci.*, in press, 1993.

B. A. Albrecht, Department of Meteorology and Earth System Science Center, The Pennsylvania State University, University Park, PA 16802.